Advances in Bioresearch
Adv. Biores., Vol 16 (4) July 2025: 45-60

Print ISSN 0976-4585; Online ISSN 2277-1573
Journal's URL:http://www.soeagra.com/abr.html
CODEN: ABRDC3
DOI: 10.15515/abr.0976-4585.16.4.4560

Advances in Bioresearch

ORIGINAL ARTICLE

Preparation and Characterization of Dolutegravir-Loaded BSA Nanoparticles

V. Deepika[1]*, S. Srinu Naik[2], G. Vijaya Charan[3]
*1 Department of Pharmacy, University College of Technology, Osmania University, Hyderabad, India.
2 Department of Chemical Engineering, University College of Technology, Osmania University, Hyderabad, India.
3 Department of Chemistry, University College of Science, Osmania University, Hyderabad, India.
***Corresponding author's email:** deepikavinugala@gmail.com

ABSTRACT
Dolutegravir (DTG), a widely used integrase strand transfer inhibitor (INSTI) for HIV treatment, is challenged by poor aqueous solubility, variable bioavailability, and systemic side effects. To address these limitations, this study developed and optimised bovine serum albumin (BSA)-based nanoparticles for the delivery of dolutegravir using the desolvation technique, guided by a Box-Behnken Design. The optimised formulation exhibited a particle size of approximately 159.7 nm, high entrapment efficiency (~80.5%), and favourable zeta potential (-26.4 mv), indicating good stability. In vitro studies demonstrated sustained drug release over 12 hours, while in vivo pharmacokinetic evaluations in rats revealed enhanced bioavailability, extended half-life (12 hours), and prolonged systemic circulation. Characterisation through FTIR, DSC, SEM, and statistical analysis confirmed the structural integrity and robustness of the nanoparticles. These findings suggest that BSA-based nanoparticles are a promising platform for dolutegravir delivery, offering potential improvements in therapeutic efficacy, reduced dosing frequency, and better patient adherence. Further research is warranted to evaluate long-term safety, in vivo efficacy, and potential clinical applications.
Keywords: *Dolutegravir, Nanoparticles, bovine serum albumin, FTIR, DSC, SEM.*

Received 19.05.2025 Revised 25.06.2025 Accepted 05.07.2025

How to cite this article:
V. Deepika, S. Srinu Naik, G. Vijaya Charan. Preparation and Characterization of Dolutegravir-Loaded BSA Nanoparticles. Adv. Biores. Vol 16 [4] July 2025.45-60

INTRODUCTION

Dolutegravir (DTG) is a second-generation integrase strand transfer inhibitor (INSTI) that plays a pivotal role in combination antiretroviral therapy (cART) for the management of Human Immunodeficiency Virus (HIV) infection. It exerts its therapeutic action by selectively inhibiting the HIV integrase enzyme, which is essential for the integration of viral DNA into the host genome—a critical and irreversible step in the viral replication cycle. By obstructing this integration, dolutegravir prevents the establishment of infection in new cells. The drug is widely endorsed by the World Health Organization (WHO) and numerous national guidelines as part of preferred first-line treatment regimens due to its high genetic barrier to resistance, robust antiviral efficacy, favorable pharmacokinetic profile, and once-daily dosing convenience. Its relatively long plasma half-life (~14 hours), low potential for drug-drug interactions, and minimal hepatic enzyme induction further enhance its clinical utility [1].

Despite its favorable therapeutic characteristics, dolutegravir is associated with certain pharmacokinetic and formulation-related limitations. Chief among these is its poor aqueous solubility, which leads to challenges in achieving optimal oral bioavailability. Additionally, dolutegravir exhibits low permeability and suboptimal penetration across the blood-brain barrier (BBB), which may restrict its accumulation in central nervous system (CNS) tissues—one of the key reservoirs for latent HIV infection [2-3]. These factors can compromise the drug's efficacy in completely eradicating viral reservoirs and achieving long-term viral suppression. Moreover, clinical reports have highlighted concerns regarding dolutegravir's association with adverse events, including neuropsychiatric symptoms (e.g., insomnia, anxiety, depression), weight gain, and metabolic alterations, particularly with chronic use.

To overcome these limitations and improve therapeutic outcomes**,** nanotechnology-based drug delivery systems are increasingly being explored. Among these, Bovine Serum Albumin (BSA) nanoparticles have garnered significant attention due to their biocompatibility, biodegradability, non-immunogenic nature, and the ability to bind and transport a wide range of pharmaceutical agents. BSA is a globular protein with natural affinity for hydrophobic drugs, making it an ideal carrier for enhancing the solubility and delivery of poorly water-soluble molecules like dolutegravir [4-8].

BSA nanoparticles offer multiple advantages over conventional formulations, including enhanced drug stability, protection against enzymatic degradation, and the potential for sustained and controlled drug release [9-12]. These features can reduce dosing frequency and improve patient adherence. Furthermore, BSA nanoparticles can be surface-functionalized with targeting moieties (e.g., folic acid, transferrin, mannose) or polyethylene glycol (PEG) chains to extend systemic circulation time, minimize clearance by the reticuloendothelial system (RES), and facilitate active targeting to specific tissues such as the brain, lymph nodes, or macrophage reservoirs. Such modifications can significantly enhance drug accumulation in latent HIV reservoirs, thereby improving the overall therapeutic efficacy and reducing systemic side effects.The application of BSA-based nanoparticles in dolutegravir delivery systems represents a promising and innovative approach to optimize HIV pharmacotherapy. By addressing solubility, stability, and targeting limitations, these nanosystems may contribute to the next generation of long-acting, patient-friendly antiretroviral regimens with the potential for better management of HIV infection and possibly functional cure strategies [13-16].

MATERIAL AND METHODS

Chemicals and Reagents:

The active pharmaceutical ingredients (APIs) were obtained as gift samples from reputed pharmaceutical companies. All other chemicals and reagents of analytical grade were procured from Oxford Lab Fine Chem LLP (Mumbai, India

Methodology

Preformulation Studies

Solubility Determination

The solubility of Dolutegravir was evaluated in distilled water and phosphate buffer (pH 7.4). An excess amount of drug was added to each solvent to form a saturated solution, which was stirred continuously for 24 hours at room temperature. The solutions were then filtered through Whatman No. 1 filter paper and the filtrates were analyzed spectrophotometrically at 258 nm to determine the drug concentration [17-19].

Melting Point Determination

The melting point of Dolutegravir was determined using Thiel's melting point apparatus. The powdered drug was placed in a capillary tube sealed at one end and heated gradually. The temperature at which the drug melted was recorded, and the average of three readings was taken to ensure accuracy.

Absorption Maxima (λmax) Determination

A standard stock solution of Dolutegravir was prepared in 0.1N HCl. The solution was scanned in the UV region from 200 to 400 nm using a UV-Visible spectrophotometer. The same procedure was repeated in phosphate buffers of pH 6.8 and 7.4 to determine the λmax in different media.

Standard Graph Preparation

A stock solution of Dolutegravir was prepared in 0.1N HCl. From this, serial dilutions were made to obtain concentrations of 2, 4, 6, 8, and 10 µg/mL. The absorbance of each solution was measured at 258 nm using a UV-Visible spectrophotometer. A calibration curve was plotted with concentration on the X-axis and absorbance on the Y-axis to ensure linearit

Preparation of BSA Nanoparticles by the Desolvation Technique

BSA nanoparticles were prepared using the desolvation technique, which involves the dropwise addition of an organic phase to an aqueous phase under controlled conditions. Initially, a 1% w/v solution of Poloxamer 188 was prepared in distilled water and stirred continuously, followed by the addition of Bovine Serum Albumin (BSA) as per the concentrations defined by the Box–Behnken Design (BBD). In parallel, the organic phase was prepared by dissolving 50 mg of the drug in ethanol at varying concentrations, followed by ultrasonication to ensure complete solubilization. The organic phase was then added slowly to the aqueous phase under continuous stirring at speeds specified by the BBD. The appearance of turbidity indicated nanoparticle formation. Subsequently, 8% v/v glutaraldehyde was added as a crosslinking agent, and the mixture was stirred continuously for 5 hours to allow for complete crosslinking and stabilization of the nanoparticles.

Optimization

The Box-Behnken Design (BBD) was used to optimize nanoparticles by analyzing the effects of BSA concentration (X1), ethanol volume (X2), and stirring speed (X3) on particle size (Y1), entrapment efficiency (Y2), and zeta potential (Y3). The design involved 17 formulation interactions and five central points. Regression analysis and ANOVA identified the best model, and 3D response surface graphs were used to compare observed and predicted results. A standard quadratic equation was derived to represent the relationships between the variables and responses [19-22].

Table 1: Design parameters for the experiment

Independent Variables(X)	**Coded Value**		
	Low (-1)	**Mid (0)**	**High (+1)**
BSA (X1) (mg)	50	100	150
Ethanol(**X2) (ml)**	10	15	20
Stirring speed **(X3) (rpm)**	500	750	1000
Responses(Y)	**Constraint**		
Particle size(Y1) Entrapment efficiency (Y2) Zeta potential (Y3)	Minimize Maximize > -20		

Preparation of Albumin Nanoparticles containing Dolutegravir

Albumin nanoparticles containing Dolutegravir are prepared using the desolvation method, which involves dissolving bovine serum albumin (BSA) in deionized water or phosphate-buffered saline and adjusting the pH to between 7.0 and 9.0. Dolutegravir is incorporated into the albumin solution either by dissolving it in ethanol or dispersing it with the aid of sonication. Ethanol is then added dropwise to the mixture under constant stirring, inducing phase separation and nanoparticle formation due to reduced albumin solubility. To stabilize the nanoparticles, glutaraldehyde is added as a crosslinker, reacting with lysine and arginine residues of albumin to form covalent bonds that enhance the structural integrity, biodegradability, and controlled drug release properties. The resulting nanoparticles are purified by centrifugation or ultrafiltration to remove unbound drug, ethanol, and excess crosslinker, and are finally resuspended or lyophilized for further use [22-25].

EVALUATION OF PREPARED NANOPARTICLES

Entrapment efficiency

Separate the free (unentrapped) drug from the encapsulated drug by centrifugation for 60 mins at 4 0 C and 15,000 rpm. This separates the nanoparticles (containing the encapsulated drug) from the free drug in the supernatant. The obtained supernatant was diluted and subsequently analyzed using spectrophotometry.

$$Entrapment\ efficiency = \frac{Total\ amount\ of\ drug - amount\ of\ free\ drug}{Total\ weight\ of\ the\ nanoparticles}$$

Vesicle size, polydispersity index (PDI), and zeta potential (ZP) analysis

The size of the vesicles and the PDIwere assessed using a zeta sizer, following the dilution of nanoparticle samples with double-distilled water in a quartz cuvette (Zetasizer Nano, Malvern, UK). The average vesicle size, polydispersity index, and zeta potential of the adjusted formulations were determined using the Zetasizer's dynamic light scattering technique following the proper sample dilution.

In-vitro drug release studies

The drug release from nanoparticles was measured using the dialysis bag method. A 2 mL sample was placed in a tightly knotted dialysis membrane, which was then submerged in 100 mL of phosphate buffer solution (pH 6.8) and stirred at 100 rpm. Samples were taken at intervals (0, 2, 3, 4, 6, 8, 10, 12 hours), with 5 mL of fresh PBS added each time. The cumulative drug release was determined by UV spectrophotometry at 258 nm.

Drug excipients compatibility studies

Fourier Transform Infrared (FTIR) Spectroscopy

The FTIR spectrophotometer's KBr disk method was used to obtain the sample spectra. To create a KBr disk, roughly 2-3 mg of the sample was combined with an equal weight of dried potassium bromide and compacted. At a resolution of 4 cm-1, the samples were scanned in the 400–4000 cm−1 spectral range.

Differential scanning calorimetry (DSC)

Thermal properties of pure drugs were studied using Differential Scanning Calorimetry (DSC), with indium as the standard. Samples (5 mg) were heated from 10 to 300°C at 10°C/min under N2 flow. For SEM, nanoparticle samples were diluted, placed on a carbon grid, air-dried, coated with chromium, and

analyzed in a vacuum chamber. Electrons emitted from the sample were detected to create high-resolution images, allowing visualization of nanoparticle morphology, surface structure, and size.

Pharmacokinetic Study of Dolutegravir BSA NP in Rats

Ten male Wistar rats (200–250 g) from Anurag University's Animal Care Facility were divided into two groups. One group received 8 mg/kg dolutegravir in 0.1% CMC, while the other received the same dose of optimized Dolutegravir-loaded BSA nanoparticles (opt-DBNP). Rats were fasted for 8-10 hours before receiving the doses via oral gavage. Blood samples were collected at various intervals, centrifuged, and plasma stored at −80°C for analysis. Dolutegravir concentration was measured using RP-HPLC with specific mobile phases, and pharmacokinetic parameters were calculated using Kinetica via non-compartmental analysis.

RESULTS AND DISCUSSION

Determination of Melting Point

The melting point of Dolutegravir was determined using the capillary method, and the observed values across three trials were consistent, with slight variation. The average melting point was found to be **192°C**, confirming the drug's purity and alignment with reported literature values

Determination of Solubility

From the results shown in Table 2, It belongs to BCS-III, so it is soluble in water and organic solvents.

Table 2: solubility profile of drug in different medium

Medium	Solubility
Ethanol	Soluble
Chloroform	Soluble
Methanol	Soluble
Water	Soluble

Determination of absorption maximum

The absorption maximum (λmax) of Dolutegravir was determined using a UV-Visible Spectrophotometer by scanning the drug solution in the wavelength range of 200–400 nm. It was observed that Dolutegravir exhibited the highest absorbance at **258 nm**, which was identified as its λmax and used for further spectrophotometric analysis.

Standard curve

Table 3: Standard curve of DLV in 0.1N HCl

Concentration(µg/ml)	Absorbance
2.0	0.2094
4.0	0.4239
6.0	0.6429
8.0	0.9107
10.0	1.1035

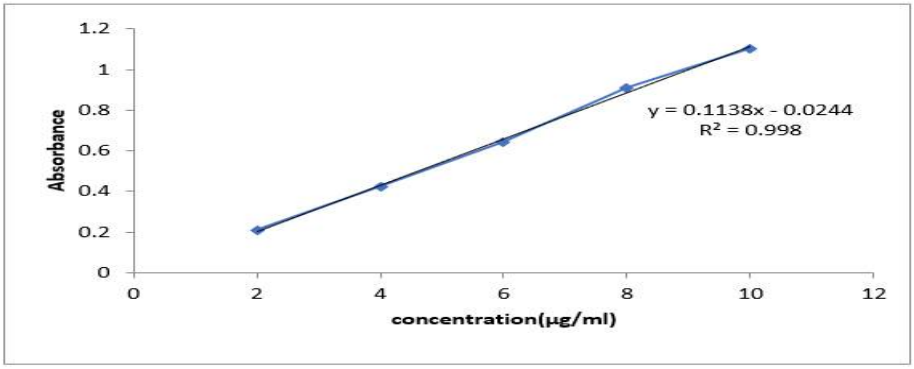

Figure 1: Calibration Curve of DLV in 0.1N HCI at 258nm

The standard curve of DLV in 0.1N HCl was constructed using concentrations ranging from 2 to 10 µg/ml, with corresponding absorbance values measured at 258 nm. A linear relationship was observed with a good correlation between concentration and absorbance, shown in Table 3 and Figure 1.

Table 4: Standard curve of DLV in 6.8 pH buffer at 258nm

Concentration(µg/ml)	Absorbance
2	0.4731
4	0.5279
6	0.6267
8	0.7048
10	0.7598

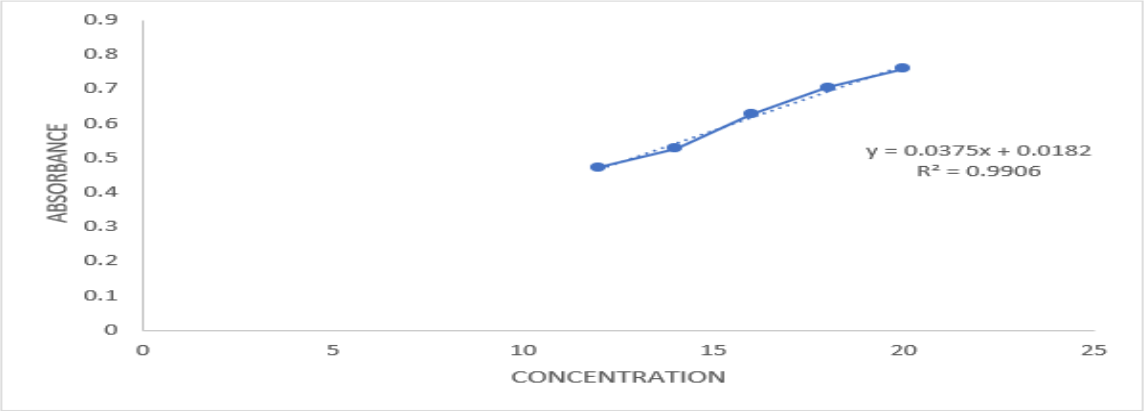

Figure 2: Calibration Curve of DLV in 6.8 pH buffer

Table 5: Standard curve of DLV in 7.4 pH buffer

Concentration(µg/ml)	Absorbance
2.0	0.0554
4.0	0.1125
6.0	0.163
8.0	0.1999
10.0	0.257

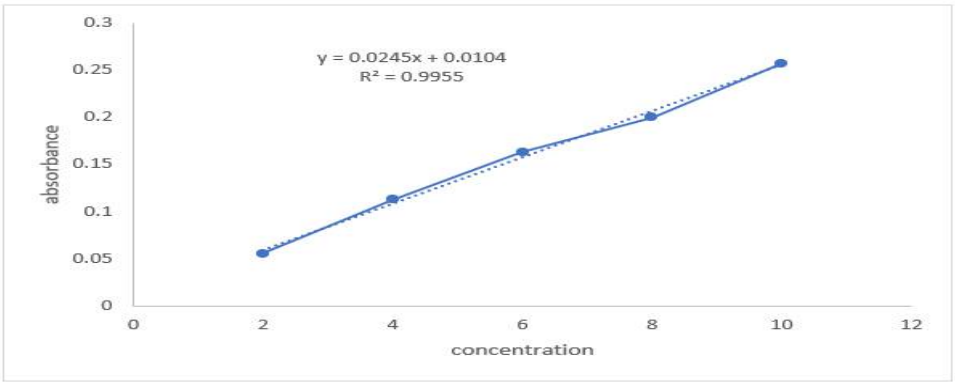

Figure 3: Calibration Curve of DLV in 7.4 pH buffer

Various concentrations were formulated in 0.1N HCl, phosphate buffers 6.8 and 7.4, and the correlation coefficients of R^2 were found to be 0.998, 0.9906, and 0.9959, individually.

FTIR Study

The FTIR spectrum of Dolutegravir confirms the presence of key functional groups consistent with its chemical structure. A broad peak at 3364.17 cm^{-1} indicates N–H stretching, corresponding to the amide groups present in the molecule. A strong absorption at 1692.47 cm^{-1} is attributed to C=O stretching vibrations of the carboxylic acid and keto functionalities. Peaks observed at 1606.43 cm^{-1} and 1572.52 cm^{-1} represent aromatic C=C stretching and N–H bending, confirming the presence of aromatic rings and amide linkages. The bands around 1454.65 cm^{-1} and 1411.26 cm^{-1} are due to C–H bending, while the peak at 1237.79 cm^{-1} corresponds to C–N stretching of amide groups. A distinct absorption at 1042.77 cm^{-1} is assigned to C–F stretching, validating the presence of fluorine atoms in the molecule. These characteristic peaks collectively support the structural identity and purity of Dolutegravir

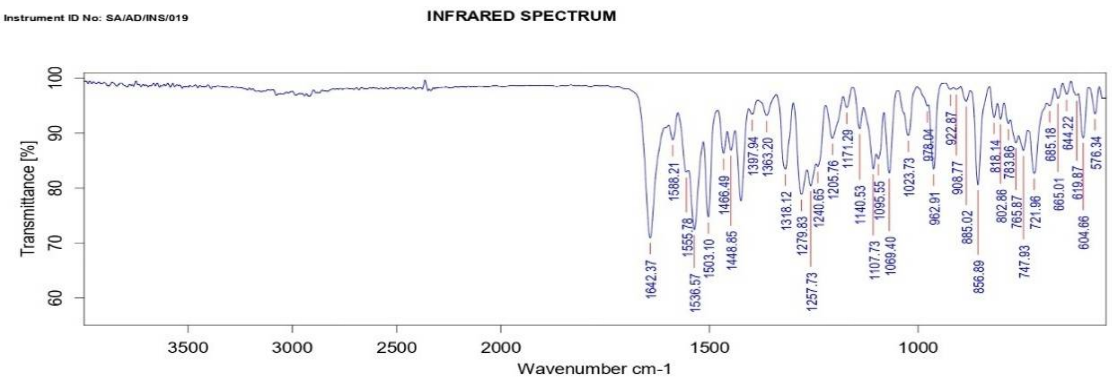

Figure 4: FTIR spectra of pure drug

DSC Report

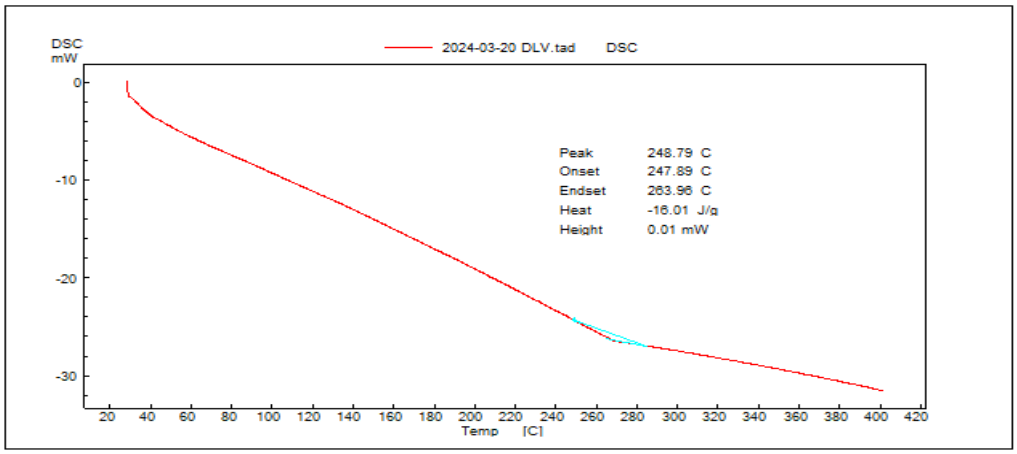

Figure 5: DSC curve of DLV

The Differential Scanning Calorimetry (DSC) analysis of Dolutegravir (DLV) reveals an endothermic peak at **248.79°C**, indicating its melting point and confirming its crystalline nature. The onset of the melting process begins at **247.89°C** and concludes at an endset temperature of **283.96°C**, demonstrating a relatively narrow melting range, which further supports the drug's purity. The enthalpy of fusion (ΔH) is calculated as **-16.01 J/g**, which corresponds to the energy required for the phase transition. This thermal behavior is characteristic of a pure, crystalline compound and aligns with standard thermal profiles of Dolutegravir shown in Figure 5.

The particle size and zeta potential

The particle size and zeta potential analysis of the Dolutegravir-loaded albumin nanoparticles revealed a Z-average particle size of **794.0 nm** with a **polydispersity index (PDI) of 1.327**, indicating a broad size distribution and moderate uniformity in the nanoparticle population. The zeta potential measurement exhibited a peak near **0 mV**, suggesting a **low surface charge**, which may lead to limited electrostatic repulsion and reduced colloidal stability. These findings imply that while the nanoparticles are within the nanometer range, their stability may require enhancement through formulation optimization or the addition of stabilizers to prevent aggregation.

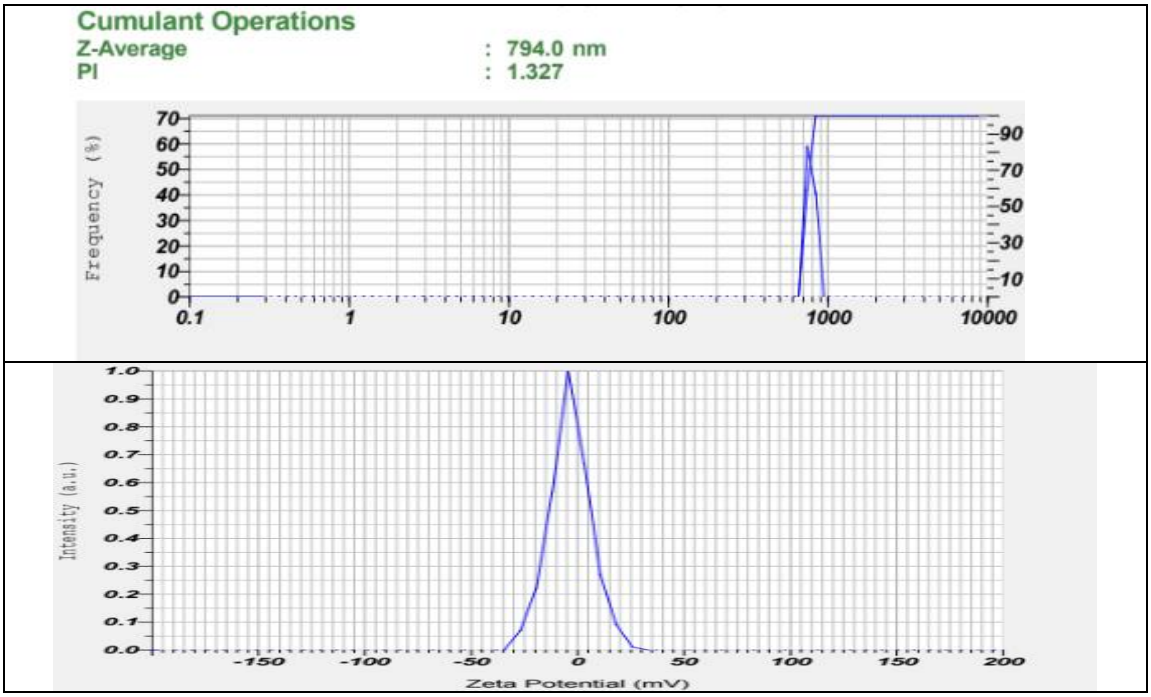

Figure 6: particle size and Zeta potential of the trial formulation

Optimization

Table 6 illustrates the formulation matrix developed using the Box-Behnken Design (BBD) for BSA-based nanoparticles loaded with a drug. The independent variables were BSA concentration (X_1), ethanol volume (X_2), and stirring speed (X_3), while the dependent responses were particle size (Y_1), entrapment efficiency (Y_2), and zeta potential (Y_3). Among the 17 experimental runs, formulations DBNP 5, DBNP 8, DBNP 9, DBNP 12, and DBNP 14 represented the central points, ensuring replication and estimation of experimental error. The high regression coefficient values indicate that the selected variables significantly influenced the responses, particularly particle size and entrapment efficiency. Optimal particle size and zeta potential values were observed in formulations with intermediate ethanol volume and stirring speed, suggesting a balanced formulation approach.

Table 6: Formulation for Drug loaded with BSA Nanoparticle using Box-Behnken Design

Formulation Code	X1 BSA (mg)	X2 Ethanol (ml)	X3 Stirring speed (rpm)	Y1 Particle size	Y2 Entrapment efficiency	Y3 Zeta potential
DBNP1	100	10	1000	162.2	70.42	-37.5
DBNP 2	50	15	500	170.9	70.76	-32.2
DBNP 3	150	20	750	161	74.68	-30
DBNP 4	50	10	750	168.9	72.3	-33.1
DBNP 5	100	15	750	156.7	70.1	-34.9
DBNP 6	50	20	750	167.8	72.3	-32.4
DBNP 7	150	15	500	163.2	67.4	-33.5
DBNP 8	100	15	750	154.4	73.3	-32.7
DBNP 9	100	15	750	158.5	69.5	-36.5
DBNP 10	150	15	1000	160.9	68.1	-30.9
DBNP 11	100	20	500	163.1	68.5	-36.6
DBNP 12	100	15	750	152.2	70.6	-30.4
DBNP 13	100	10	500	162.9	68.8	-35.1
DBNP 14	100	15	750	157	69	-31.2
DBNP 15	150	10	750	163	71.9	-38.2
DBNP 16	50	15	1000	170.6	66.12	-26
DBNP 17	100	20	1000	164.6	71.30	-40.1

Statistical Analysis & Optimization Study

Model Validation

The ANOVA results in Table 7 confirm that the quadratic model is statistically significant ($\boldsymbol{p}$ = 0.0028), indicating a good fit for predicting particle size. BSA (X1) showed a significant effect ($\boldsymbol{p}$ = 0.0017), while

ethanol (X2) and stirring speed (X3) were not significant. Interaction terms were also non-significant, suggesting minimal combined effects. However, the quadratic terms $X1^2$, $X2^2$, and $X3^2$ were all significant, indicating non-linear influences. The non-significant lack of fit (***p*** = 0.7306) confirms the model's adequacy and reliability.

Table 7: Model validation by Anova for Quadratic Model (Response 1: *Particle size (nm)*)

Source	Sum of Squares	df	Mean Square	F-value	p-value	
Model	433.42	9	48.16	10.30	0.0028	significant
X1-BSA	113.25	1	113.25	24.23	0.0017	
X2-Ethanol	0.0313	1	0.0313	0.0067	0.9371	
X3-Stirring Speed	0.4050	1	0.4050	0.0866	0.7770	
X1X2	0.2025	1	0.2025	0.0433	0.8410	
X1X3	1.0000	1	1.0000	0.2139	0.6577	
X2X3	1.21	1	1.21	0.2589	0.6265	
$X1^2$	167.51	1	167.51	35.84	0.0005	
$X2^2$	40.66	1	40.66	8.70	0.0214	
$X3^2$	79.03	1	79.03	16.91	0.0045	
Residual	32.72	7	4.67			
Lack of Fit	8.27	3	2.76	0.4508	0.7306	not significant
Pure Error	24.45	4	6.11			
Cor Total	466.14	16				

ANOVA of Quadratic Model for Response 1 Particle size

The highest-order polynomial was used to avoid aliasing, with a significant F-value of 2.00 ($P < 0.05$). Key terms (A, B, C, AC, BC, A^2, B^2, C^2) were significant, while terms with $P > 0.1$ may be removed to improve model efficiency.

Y1=155.76-3.76X1-0.0625X2-0-2250X3-2250X1X2-0.5000X1X3+0.5000X2X3+6.31X12 +3.11X22+4.33X32

The reaction at specific amounts of each element can be predicted using the equation stated in terms of coded factors. High and low levels of the components are commonly represented by the symbols +1 and -1, respectively. By examining the coefficients connected to each component, this coded equation provides a useful tool for determining the relative importance of the elements.

Effect of independent variables on Particle Size (Y1)

Particle size is influenced by BSA concentration, ethanol volume, and stirring speed. Lower BSA, higher ethanol, and higher speed produce smaller, more uniform particles with better stability. High BSA or low ethanol increases size and heterogeneity (high PDI). These interactions help optimize formulation for stable, uniform nanoparticles in pharmaceutical use.

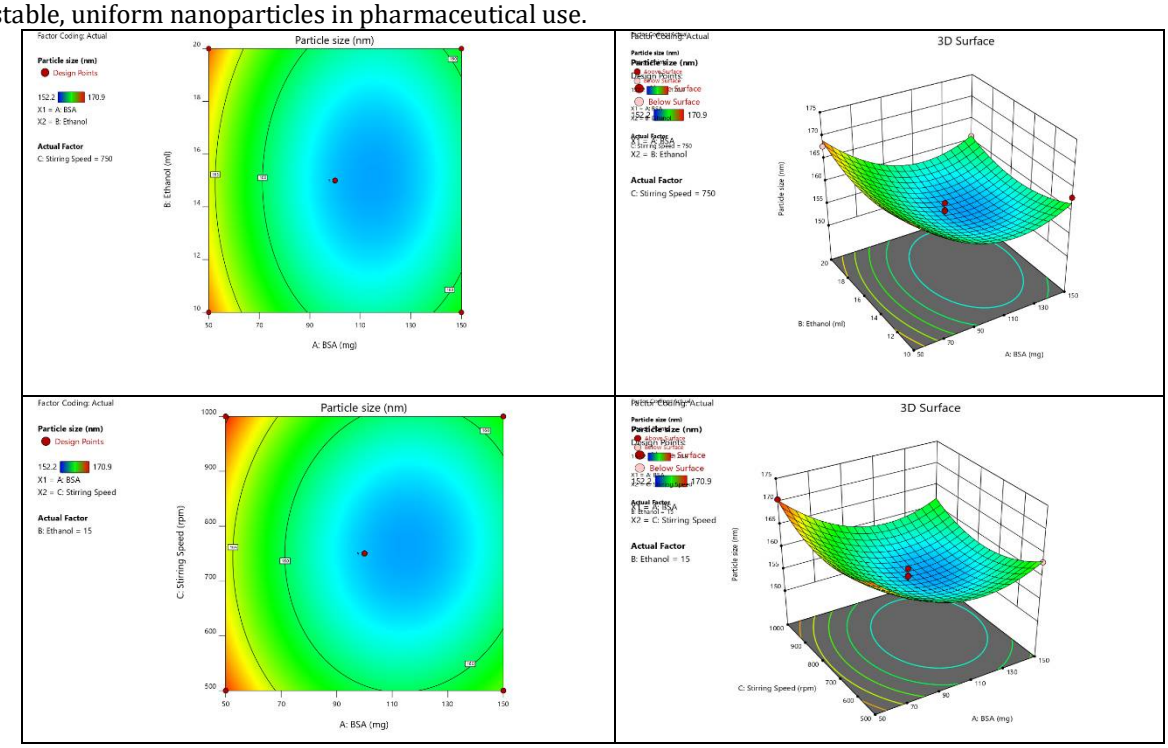

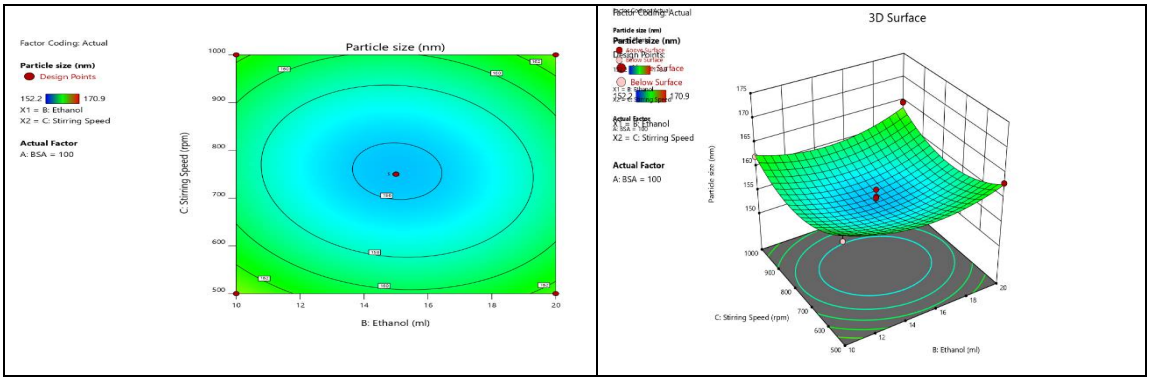

Figure 7: 2D Contour plot &3D simulation curve *Effect of Independent variables on particle size*

Table 8: Model validation by Anova for Quadratic Model (Response 2: EE)

Source	Sum of Squares	Df	Mean Square	F-value	p-value	
Model	56.63	9	6.29	2.00	0.1863	significant
X1-BSA	0.0450	1	0.0450	0.0143	0.9081	
X2-Ethanol	1.41	1	1.41	0.4488	0.5244	
X3-Stirring Speed	0.0288	1	0.0288	0.0092	0.9264	
X1X2	1.93	1	1.93	0.6144	0.4588	
X1X3	7.13	1	7.13	2.27	0.1759	
X2X3	0.3481	1	0.3481	0.1107	0.7491	
$X1^2$	0.4244	1	0.4244	0.1350	0.7242	
$X2^2$	16.47	1	16.47	5.24	0.0560	
$X3^2$	31.21	1	31.21	9.92	0.0161	
Residual	22.01	7	3.14			
Lack of Fit	10.75	3	3.58	1.27	0.3967	not significant
Pure Error	11.26	4	2.81			
Cor Total	78.64	16				

ANOVA of Quadratic Model for Response 2 Entrapment efficiency

The highest-order polynomial model was chosen to avoid aliasing, with an F-value of 2.00 indicating significance ($P < 0.05$). Key terms (A, B, C, AC, BC, A^2, B^2, C^2) were significant, while terms with $P > 0.1$ may be excluded to improve the model. A non-significant lack of fit (F = 0.50, P = 39.67%) confirms the model's validity.

Y2=70.50+0.0750X1+0.4200X2-00.0600X3-0.6950X1X2+1.33X1X3+0.2950X2X3+0.3175X12 +1.98X22-2.72X32

The reaction at specific amounts of each element can be predicted using the equation stated in terms of coded factors. High and low levels of the components are commonly represented by the symbols +1 and -1, respectively. By examining the coefficients connected to each component, this coded equation provides a useful tool for determining the relative importance of the elements.

Effect of independent variables on Entrapment Efficiency (Y2)

Entrapment efficiency (EE) is influenced by BSA concentration, ethanol volume, and stirring speed. Moderate BSA levels and higher ethanol volumes improve EE, but excessive amounts may reduce it due to particle instability or size. Higher speed enhances EE by creating smaller, uniform particles, though overly high speed may degrade the matrix. Optimal EE is achieved by balancing these factors for efficient drug encapsulation.

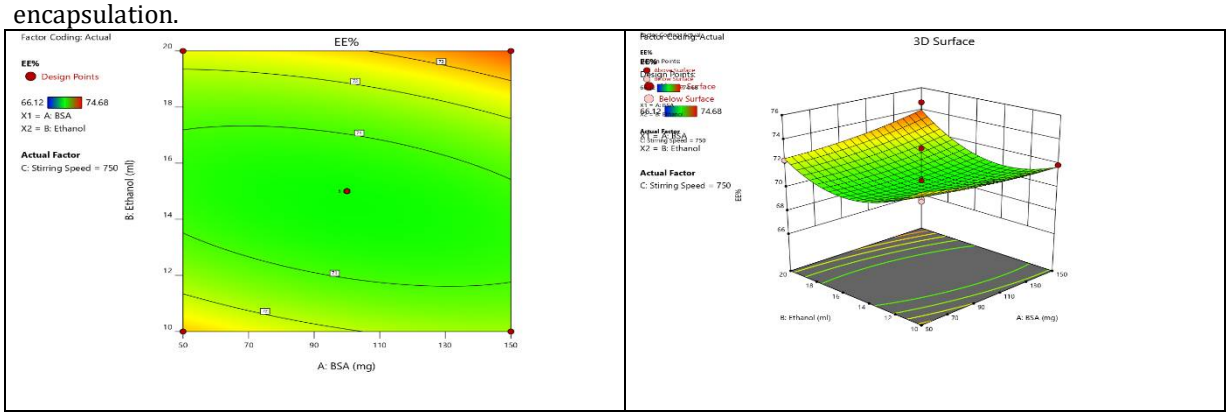

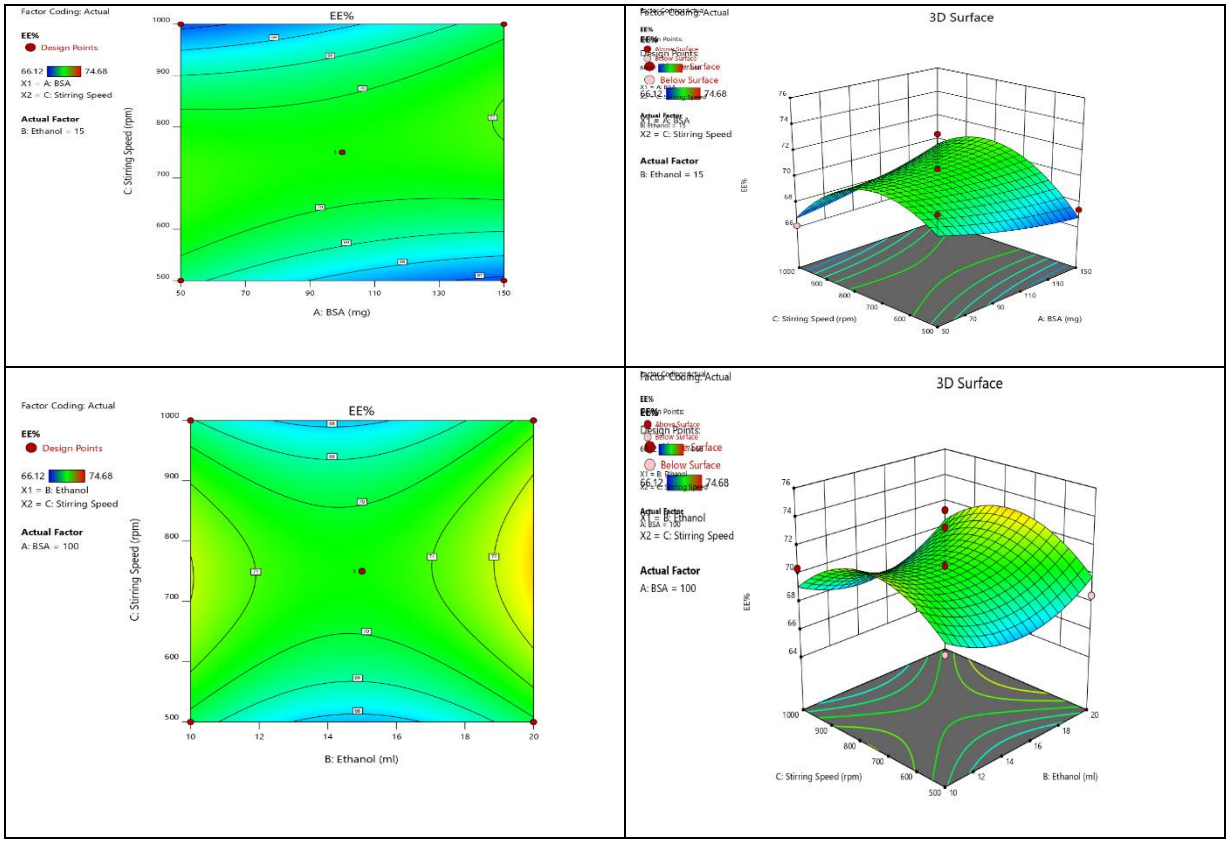

Figure 8: 2D Contour plot & 3D simulation curve Effect of Independent variables on Entrapment Efficiency %

Table 9: Model validation by Anova for Quadratic Model (Response 3: ZP)

Source	Sum of Squares	df	Mean Square	F-value	p-value	
Source	**Sum of Squares**	**df**	**Mean Square**	**F-value**	**p-value**	
Model	122.93	9	13.66	1.27	0.3864	significant
X1-BSA	9.90	1	9.90	0.9178	0.3700	
X2-Ethanol	2.88	1	2.88	0.2670	0.6213	
X3-Stirring Speed	1.05	1	1.05	0.0974	0.7640	
X1X2	14.06	1	14.06	1.30	0.2911	
X1X3	3.24	1	3.24	0.3003	0.6007	
X2X3	0.3025	1	0.3025	0.0280	0.8718	
$X1^2$	42.98	1	42.98	3.98	0.0861	
$X2^2$	50.99	1	50.99	4.73	0.0662	
$X3^2$	2.09	1	2.09	0.1940	0.6729	
Residual	75.52	7	10.79			
Lack of Fit	49.67	3	16.56	2.56	0.1928	not significant
Pure Error	25.85	4	6.46			
Cor Total	198.45	16				

ANOVA of Quadratic Model for Response 3 Zeta Potential

The highest-order polynomial model was chosen to ensure significance and avoid aliasing. With an F-value of 1.27 and a 0.01% chance due to noise, key terms (A, B, C, AC, BC, A^2, B^2, C^2) were significant ($P < 0.05$). Non-significant terms ($P > 0.1$) may be removed to improve performance. Coefficients reflect response changes per factor unit, while VIFs under 10 indicate acceptable multicollinearity.

Y3=-33.14-1.11X1+0.6000X2+0.3625X3-+1.87X1X2-0.9000X1X3-0.2750X2X3+0.319X12 -3.48X22-0.7050X32

Effect of Independent variables on Zeta potential (Y3)

Zeta potential was influenced by BSA concentration, ethanol volume, and stirring speed. Lower BSA levels, higher ethanol volumes, and longer stirring speed improved colloidal stability by increasing zeta potential. These conditions reduced aggregation and enhanced particle dispersion. The Box-Behnken

design highlighted how these factors individually and interactively affect stability, aiding formulation optimization.

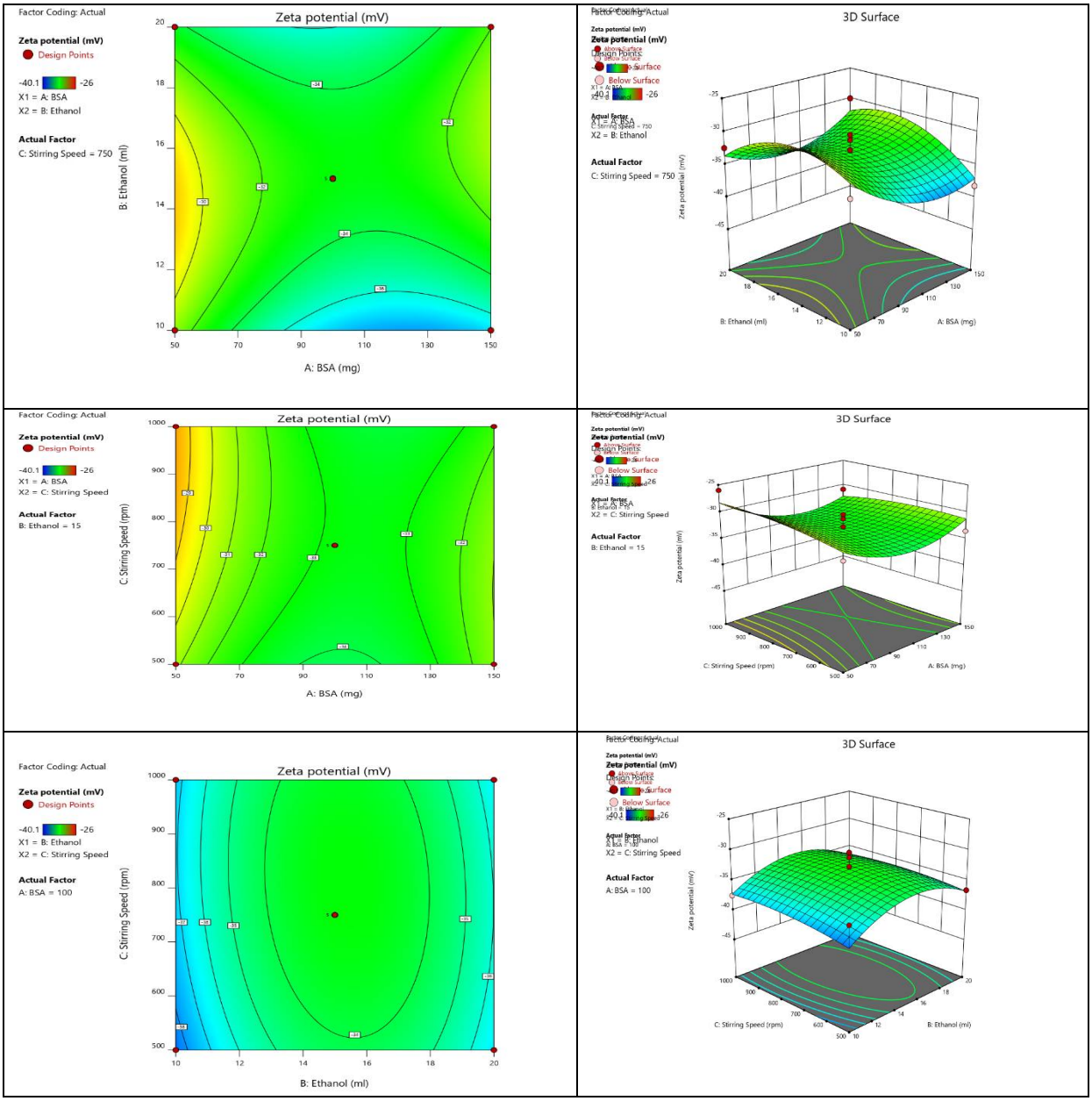

Figure 9: 2D Contour plot & 3D simulation curve *Effect of Independent variables on Zeta potential* Desirability

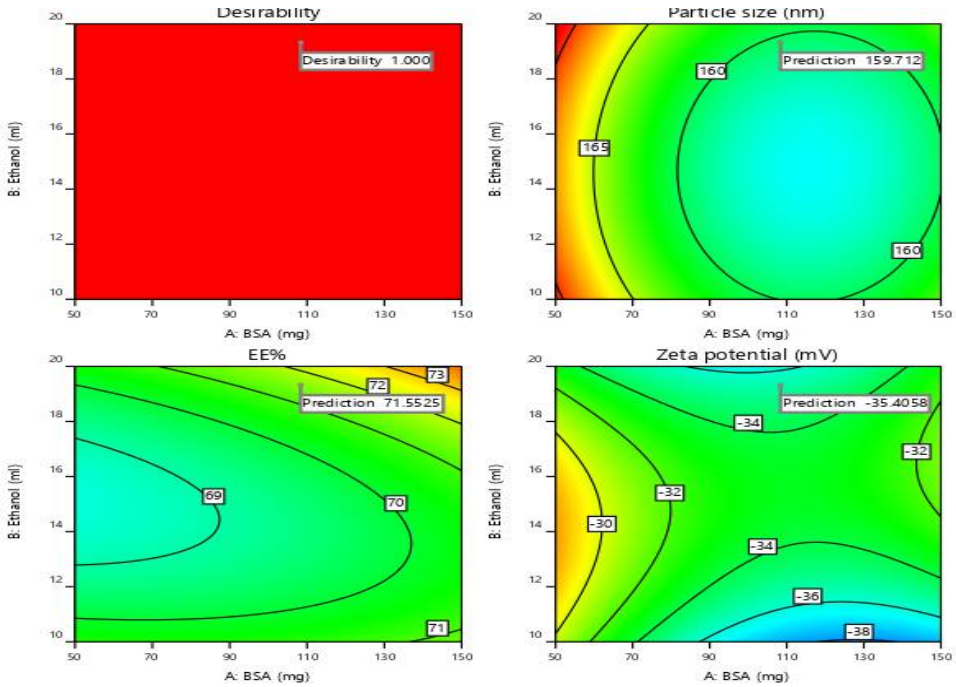

Figure 10: Desirability layout

Table 10: Point of Prediction & % of Error

Response Variable	Predicted values	Observed values	% Error
Particle size(Y1)	159.71	165.2	3.4
Entrapment efficiency (Y2)	80.55	79.10	1.80
Zeta Potential (Y3)	-26.40	-25.5	3.40
% Error=Predicted value-Observed value/ Predicted value×100 (% Error < ± 5%)			

***In vitro* drug release studies**

The drug release profile comparison between pure drug dispersion and optimized drug-loaded BSA nanoparticles (Opt-DBNP) reveals a significant difference in release behavior. The pure drug dispersion exhibited a rapid release, with 98% of the drug released within 8 hours, indicating a burst and less controlled pattern. In contrast, the Opt-DBNP formulation demonstrated a more controlled and sustained release, with 99% release achieved over 12 hours. This extended release is likely attributed to the diffusion-controlled mechanism and strong drug–polymer interactions within the nanoparticle matrix, suggesting enhanced therapeutic potential and better drug bioavailability over time, shown in Table 11.

Table 11: Cumulative percent of drug release from pure dispersion and loaded nanoparticles

Time	Pure-Drug-Dispersion	Opt-DBNP
0	0	0
2	20	15
3	42	35
4	67	55
6	79	72
8	98	85
10		92
12		99

Solid State Characterization

Physical Mixture

FTIR Analysis

Fourier Transform Infrared (FTIR) spectroscopy was conducted to evaluate the chemical integrity and potential interactions among the formulation components. Figure 11 represents the FTIR spectrum of Poloxamer 188, showing characteristic peaks corresponding to –OH stretching, C–H stretching, and C–O–C stretching vibrations. Figure 12 displays the spectrum of Glutaraldehyde, highlighting peaks typical of aldehyde groups, including C=O and C–H bending. Figure 13 presents the FTIR spectrum of Bovine Serum

Albumin (BSA), with distinct amide I and amide II bands indicative of protein structure. Figure 14 illustrates the spectrum of the physical mixture, where all major peaks of the individual components are retained without significant shifting or disappearance, confirming the absence of strong chemical interactions and the physical nature of the mixture. This supports the compatibility of components within the nanoparticle formulation.

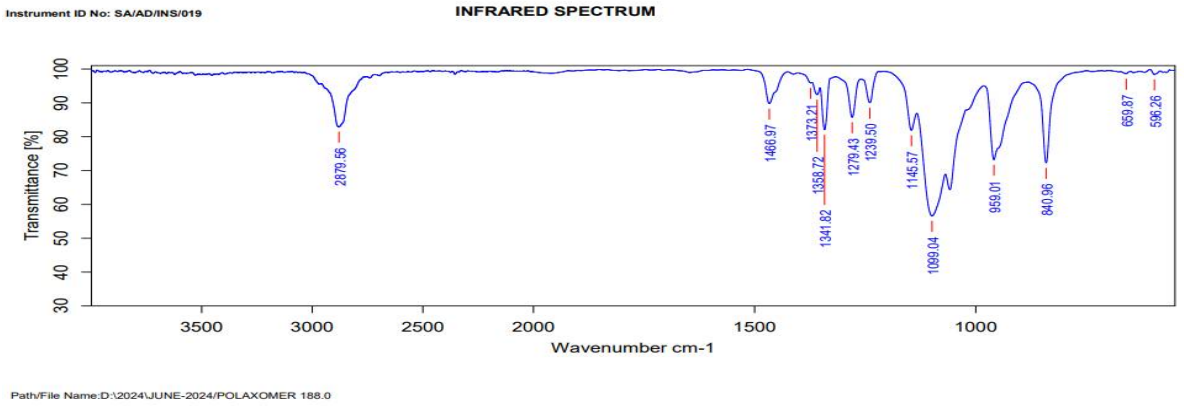

Figure 11: FTIR spectrum of Poloxamer 188

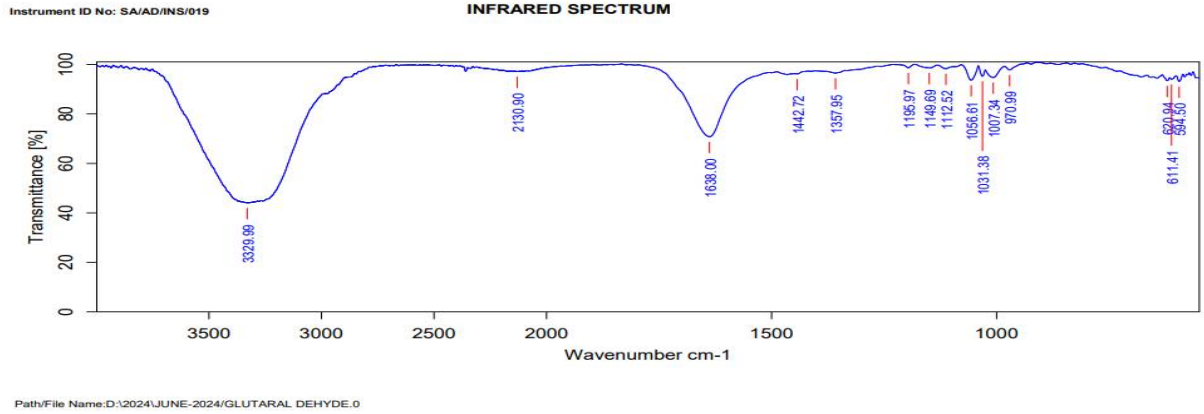

Figure 12: FTIR spectrum of Glutaraldehyde

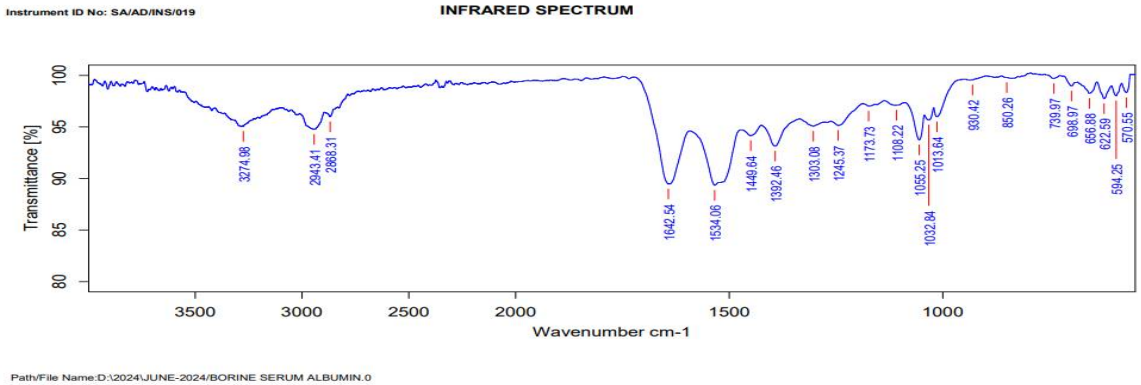

Figure 13: FTIR spectrum of Bovine Serum Albumin

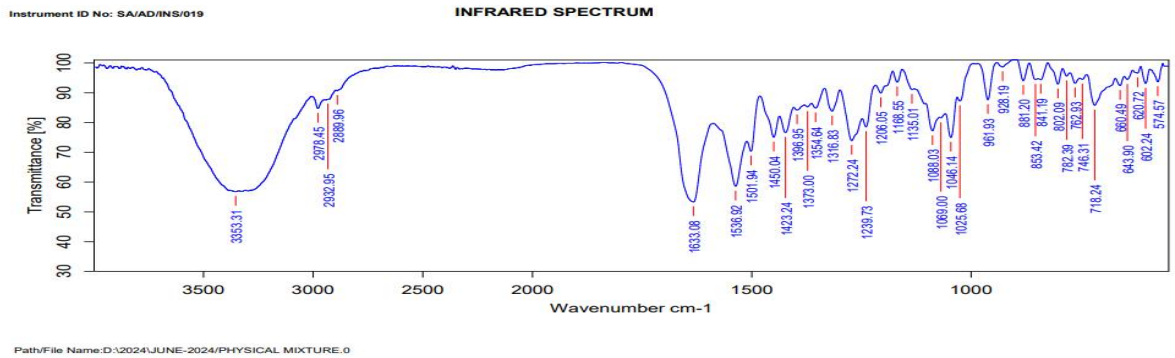

Figure 14: FTIR spectrum of Physical Mixture

Particle size and Zeta Potential of Optimized Formulation (description)

The optimized nanoparticles exhibited a uniform particle size distribution with an average size indicating nanoscale range. The zeta potential was found to be sufficiently negative, confirming good electrostatic stability. These results suggest effective formulation parameters ensuring dispersion stability and consistency in particle behavior shown in figure 15.

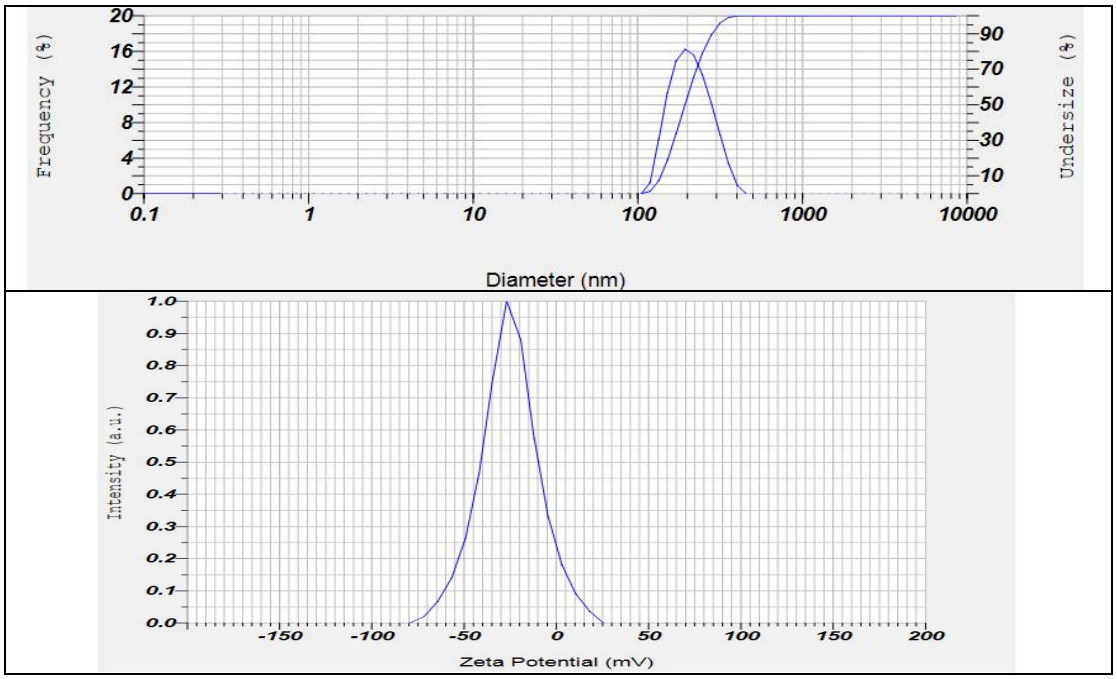

Figure 15: Particle size and Zeta Potential of Optimized Formulation

Scanning electron microscopy (SEM)

The SEM images demonstrated that the optimized albumin nanoparticles were predominantly smooth, spherical, and uniformly distributed, signifying a well-optimized and stable formulation. A few particles exhibited slight morphological deviations, appearing quasi-spherical, which could be attributed to minor aggregation or drying effects during sample preparation,The uniform surface morphology suggests effective encapsulation and minimal surface drug crystallization. These findings support the successful preparation of nanoparticles suitable for controlled drug delivery applications. shown in Figure 16.

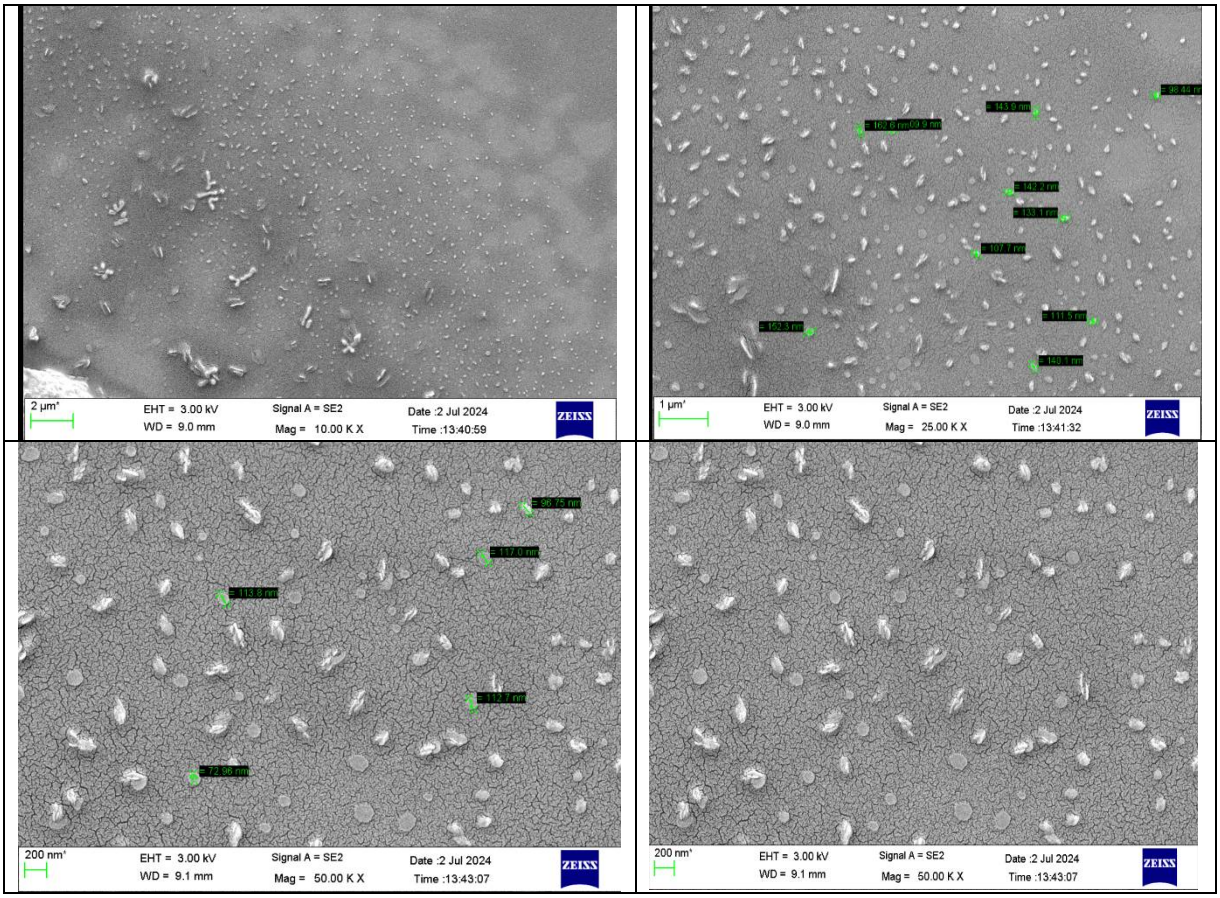

Figure 16: Scanning electron microscopy (SEM) images of Optimized Formulation

SEM images revealed that the albumin nanoparticles were mostly smooth, spherical, and uniform, indicating successful formulation. Minor shape irregularities were observed in a few particles, appearing quasi-spherical.

CONCLUSION

This study developed and optimized Dolutegravir-loaded BSA nanoparticles using the desolvation method and Box-Behnken Design. Optimized nanoparticles (~159.7 nm) showed high entrapment efficiency (~80.5%) and good stability (zeta potential -26.4 mV). They provided sustained drug release over 12 hours and enhanced intestinal absorption. Pharmacokinetic studies in rats revealed improved bioavailability, prolonged half-life (12.03 h), and sustained plasma levels. FTIR, DSC, SEM, and statistical analyses confirmed formulation integrity and robustness. This study successfully developed optimized Dolutegravir-loaded BSA nanoparticles with improved encapsulation, sustained release, and enhanced pharmacokinetics. These nanoparticles offer a promising drug delivery system by improving stability, reducing dosing frequency, and enhancing patient compliance. Future work should focus on in vivo efficacy and clinical translation.

REFERENCES

1. Elzoghby AO, Samy WM, Elgindy NA (2012). Albumin-based nanoparticles as potential controlled release drug delivery systems. J Control Release.;157(2):168–82.
2. Weber C, Coester C, Kreuter J, Langer K. (2000). Desolvation process and surface characterisation of protein nanoparticles. Int J Pharm.;194(1):91–102.
3. Langer K, Balthasar S, Vogel V, Dinauer N, von Briesen H, Schubert D. (2003); Optimization of the preparation process for human serum albumin (HSA) nanoparticles. Int J Pharm. 257(1–2):169–80.
4. Kratz F. (2008). Albumin as a drug carrier: Design of prodrugs, drug conjugates and nanoparticles. J Control Release.;132(3):171–83.
5. Wacker M. (2013). Nanocarriers for intravenous injection – The long hard road to the market. Int J Pharm.;457(1):50–62.
6. Lomis N, Westfall S, Farahdel L, Malhotra M, Prakash S, Ramakrishna S. (2016). Human serum albumin as a versatile platform for drug delivery and biosensor applications. Mater Sci Eng C.;70(Pt 1):142–9.
7. Sharma A, Sharma US. (1997). Liposomes in drug delivery: Progress and limitations. Int J Pharm.;154(2):123–40.

8. Rhaese S, von Briesen H, Ried M, Gardner CR, Kreuter J. (2003). Plasma protein (albumin) coated nanoparticles for drug targeting: Influence of receptor ligand on surface characteristics and particle size. J Microencapsul.;20(4):375–84.
9. Aggarwal P, Hall JB, McLeland CB, Dobrovolskaia MA, McNeil SE. (2009). Nanoparticle interaction with plasma proteins as it relates to particle biodistribution, biocompatibility and therapeutic efficacy. Adv Drug Deliv Rev.;61(6):428–37.
10. Balthasar S, Michaelis K, Dinauer N, von Briesen H, Kreuter J, Langer K. (2005). Preparation and characterization of antibody modified gelatin nanoparticles as drug carrier system for uptake in lymphocytes. Biomaterials.;26(15):2723–32.
11. Calvo P, Remuñán-López C, Vila-Jato JL, Alonso MJ. (1997). Novel hydrophilic chitosan–polyethylene oxide nanoparticles as protein carriers. J Appl Polym Sci.;63(1):125–32.
12. Langer K, Sadick H, Ramge P, Kramer KD, Kühn J, Schilling L, et al. (2002). Physicochemical characterization of nanoparticles designed for drug delivery to the brain. J Control Release.;83(2):403–15.
13. Kouchakzadeh H, Safarian S. (2015). Bovine serum albumin nanoparticles as controlled release carrier for 5-fluorouracil: formulation and in vitro study. Jundishapur J Nat Pharm Prod.;10(3):e23570.
14. Panyam J, Labhasetwar V. (2003). Biodegradable nanoparticles for drug and gene delivery to cells and tissue. Adv Drug Deliv Rev.;55(3):329–47.
15. Cheng YH, He C, Ruan S, He Q, Gao H. (2014). Optically and magnetically dual responsive nanoparticles for brain-targeted drug delivery. J Mater Chem B.;2(4):603–11.
16. Reddy LH, Couvreur P. (2008). Novel approaches to deliver gemcitabine to cancers. Curr Pharm Des.;14(11):1124–37.
17. You JO, Auguste DT. (2009). Nanocarrier cross-linking density and pH sensitivity regulate intracellular gene transfer. Nano Lett.;9(12):4467–73.
18. Shukla R, Bansal V, Chaudhary M, Basu A, Bhonde RR, Sastry M. (2005). Biocompatibility of gold nanoparticles and their endocytotic fate inside the cellular compartment: a microscopic overview. Langmuir.;21(23):10644–54.
19. Mahmoudi M, Simchi A, Imani M, Häfeli UO. (2009). Superparamagnetic iron oxide nanoparticles with rigid cross-linked polyethylene glycol fumarate coating for application in imaging and drug delivery. J Phys Chem C.;113(19):8124–31.
20. Sadeghi AMM, Dorkoosh FA, Avadi MR, Saadat P, Rafiee-Tehrani M. (2015). Preparation, characterization and antibacterial activities of chitosan, BSA nanoparticles loaded with isoniazid. Nanomed J.;2(1):33–40.
21. Srivastava A, Bhardwaj A, Singh S. (2013). Albumin nanoparticles as carriers for the delivery of hydrophobic drugs. Int J Pharm Sci Res.;4(3):1080–6.
22. Sahin TK, Alpsoy A. (2021). Preparation and evaluation of curcumin-loaded bovine serum albumin nanoparticles with antioxidant and antibacterial properties. J Drug Deliv Sci Technol.;61:102221.
23. Weber C, Kreuter J, Langer K. (2000). Desolvation process and surface characterization of protein nanoparticles. Int J Pharm.;194(1):91–102.
24. Muthu MS, Leong DT, Mei L, Feng SS. (2014). Nanotheranostics—application and further development of nanomedicine strategies for advanced theranostics. Theranostics.;4(6):660–77.
25. Anwer MK, Ahmed MM, Aldawsari MF, Alsaidan OA, Alsaidan MM, Alshetaili AS, et al. (2020). Fabrication of bovine serum albumin nanoparticles for efficient delivery of ciprofloxacin: a strategy for overcoming bacterial resistance. J Drug Deliv Sci Technol.;60:102091.